CORA Cork Open Research Archive
Cartlann Taighde Oscailte Chorcaí

Title	Facile electrochemical synthesis of Pd nanoparticles with enhanced electrocatalytic properties from surfactant-free electrolyte
Authors	Hasan, Maksudul;Khunsin, Worawut;Mavrokefalos, Christos K.;Maier, Stefan A.;Rohan, James F.;Foord, John S.
Publication date	2017-12-20
Original Citation	Hasan, M., Khunsin, W., Mavrokefalos, C. K., Maier, S. A., Rohan, J. F. and Foord, J. S. (2017) 'Facile Electrochemical Synthesis of Pd Nanoparticles with Enhanced Electrocatalytic Properties from Surfactant-Free Electrolyte', ChemElectroChem, In Press, doi: 10.1002/celc.201701132
Type of publication	Article (peer-reviewed)
Link to publisher's version	10.1002/celc.201701132
Rights	© 2018 Wiley-VCH Verlag GmbH & Co. KGaA, Weinheim. This is the peer reviewed version of the following article: Facile Electrochemical Synthesis of Pd Nanoparticles with Enhanced Electrocatalytic Properties from Surfactant-Free Electrolyte, ChemElectroChem, which has been published in final form at http://dx.doi.org/10.1002/celc.201701132. This article may be used for non-commercial purposes in accordance with Wiley Terms and Conditions for Self-Archiving.
Download date	2026-11-16 09:21:47
Item downloaded from	https://hdl.handle.net/10468/5239

UCC
University College Cork, Ireland
Coláiste na hOllscoile Corcaigh

FUNDAMENTALS & APPLICATIONS

CHEMELECTROCHEM

ANALYSIS & CATALYSIS, BIO & NANO, ENERGY & MORE

Accepted Article

Title: Facile Electrochemical Synthesis of Pd Nanoparticles with Enhanced Electrocatalytic Properties from Surfactant-Free Electrolyte

Authors: Maksudul Hasan, Worawut Khunsin, Christos K Mavrokefalos, Stefan A Maier, James F Rohan, and John S Foord

This manuscript has been accepted after peer review and appears as an Accepted Article online prior to editing, proofing, and formal publication of the final Version of Record (VoR). This work is currently citable by using the Digital Object Identifier (DOI) given below. The VoR will be published online in Early View as soon as possible and may be different to this Accepted Article as a result of editing. Readers should obtain the VoR from the journal website shown below when it is published to ensure accuracy of information. The authors are responsible for the content of this Accepted Article.

To be cited as: *ChemElectroChem* 10.1002/celc.201701132

Link to VoR: http://dx.doi.org/10.1002/celc.201701132

A Journal of

ChemPubSoc Europe

WILEY-VCH

www.chemelectrochem.org

WILEY-VCH

ARTICLE

Facile Electrochemical Synthesis of Pd Nanoparticles with Enhanced Electrocatalytic Properties from Surfactant-Free Electrolyte

Maksudul Hasan,*[a,b] Worawut Khunsin,[c] Christos K. Mavrokefalos,[a] Stefan A. Maier,[c] James F. Rohan,[b] and John S. Foord[a]

Abstract: Synthesis of low-dimension metallic nanoparticles of clean surface with high dispersibility and enhanced atomic surface distribution is extremely important since these strongly influence the electrocatalytic properties of the nanoparticles. In this study, the early stage electrochemical nucleation and growth of palladium nanoparticles (Pd NPs) under potentiostatic control has been investigated on a Au(111) textured substrate. The size distribution and structural characterisation of the ex-situ as-deposited Pd NPs by means of high resolution Field Emission Gun-Scanning Electron Microscopy (FEG-SEM) at different stages combined with the electrochemical measurements revealed that cluster of nuclei grew independently by the reduction of metal ions. The electrodeposited Pd NPs were very pure as confirmed by X-ray Photoelectron Spectroscopy (XPS) due to the surfactant-free green electrodeposition process and highly dispersed with an average particle size 2-5 nm. The average nanoparticle size becomes smaller with higher overpotential for the same deposition time. The synthesised Pd NPs demonstrated the largest specific surface area (4 times of commercial Pd-C) and the electrocatalytic activity in ferrocyanide/ferricyanide redox and ethanol electrooxidation processes (35 times of commercial Pd-C). This work represents an important step in achieving the fundamental understanding of nucleation and growth of nanoparticles correlating the electrocatalytic performances.

1. Introduction

Noble metal nanoparticles (NPs), usually in the size range of 10 nm and below exhibit superior electrocatalytic and electronic properties to their bulk counterparts due to unique shape, size and surface morphology.[1] Palladium (Pd) NPs have received considerable interest in recent years due to their application in various electrocatalytic processes such as in organic synthesis,[2] pharmaceuticals,[3] hydrogenation of polyunsaturated hydrocarbons,[4] hydrogen storage,[5] bio/electrochemical sensors,[6] cancer treatment,[7] fuel cells[8] and co-catalysts in photocatalysis and carbon dioxide (CO_2) reduction.[9] A recent review article has presented different synthetic methods, dimensional and morphological effects and related electrochemical applications of nanostructured Pd and Pd based materials in electrooxidation of liquid fuels, hydrogen production and storage and electrochemical sensors.[10] Controlling the shape or surface of metal NPs is crucial to their exploitation in specific applications from catalysis to chemical sensing to drug manufacturing.[1a-c, 11] To date, various synthetic approaches such as the reduction of metal salts or the decomposition of organometallic compounds have been investigated as feasible routes to the synthesis of noble metal NPs.[12] Organic functional reagents such as polymers, surfactants and ionic liquids are generally used in these wet chemical syntheses to control the morphology, dispersibility and stabilisation of NPs in the homogeneous solution phase. The actual size of synthetic NPs varies from method to method since the final formation is not controlled by a single parameter, but instead the complex and combined effects of the surfactant, reducing agent, solvent, species concentrations, temperature and reaction time.

Another popular approach is known as seed-mediated growth, in which target NPs are grown from a solution of seeding NPs of a given crystallite or shape, metal precursor salt and a mild reducing agent.[13] The seeding NPs reduce the metal species at the surface/solution interface with the help of a reducing agent. Recently, it has been reported that upon deposition ad-atoms may not remain on the same crystallite planes where deposition occurred but move to other crystallite planes due to self-surface diffusion processes.[14] This phenomenon often disrupts the growth mode and hence, the final shape or morphology of the NPs. Although homogeneous dispersion of Pd NPs has been achieved in the seeding strategies or in some of the wet chemical synthetic methods referred to above, the capability to synthesise well-defined shape and highly dispersed Pd NPs of sub 10 nm dimensions is yet to be achieved. Additionally, advanced electrocatalysis/electroanalysis based on Pd requires Pd NPs in the conductive thin film format to miniaturise the overall electrode and device dimension particularly for handheld and portable devices. In particular, there has been increasing interest in the complementary metal-oxide-semiconductor (CMOS) compatible electrodeposition method that meets the underlined demand of synthetic Pd NPs with high dispersibility, large surface-to-volume ratio and enhanced atomic surface distribution. Among these, a direct electrodeposition method based on a sacrificial anode has been demonstrated to synthesise size-selective Pd NPs in an organic electrolyte.[15] Under an applied current or potential, the bulk metallic Pd at the anode is dissolved as Pd^{2+} ions, which then migrate/diffuse to the cathode where they are reduced as ad-

[a] Dr M. Hasan, Dr C. K. Mavrokefalos, Professor J. S. Foord
Department of Chemistry, Chemistry Research Laboratory
University of Oxford
Mansfield Road, Oxford, OX1 3TA, England, UK
E-mail: maksudul.hasan@chem.ox.ac.uk
[b] Dr M. Hasan, Dr J. F. Rohan
Tyndall National Institute
University College Cork
Lee Maltings, Cork, Ireland
[c] Dr W. Khunsin, Professor S. A. Maier
Department of Physics
Imperial College London
London SW7 2AZ, England, UK

Supporting information for this article is given via a link at the end of the document

Accepted Manuscript

This article is protected by copyright. All rights reserved.

atoms. The size of the NPs can be controlled via a number of parameters such as solvent polarity, current density, charge flow, distance between electrodes, etc.[15b] This method was then further improved by the direct electroreduction of metal precursor salts in aqueous electrolytes i.e., metallic ions are directly provided by electrolyte rather than the sacrificial anode.[16] Despite the improvement, there exists an inherent drawback with the method, i.e. two competitive processes occurring at the cathode; one is the reduction of metal ions as NPs and other is the reduction as a metallic film.[17] To shift the balance in favour of NPs growth a surfactant is typically used to enhance the rate of NPs formation rather than the metallic thin film deposition. Also, the use of an ideal surfactant is crucial in stabilising the metal ions as nanocluster in the solution phase, which prevents precipitation as solid metal before the ions reach the cathode. The molecular nature of the surfactant, however, strongly affects the size and dispersibility of the synthesised metallic NPs. Moreover, it is not always possible to find a suitable surfactant for the specific size-selective synthesis of metal NPs.

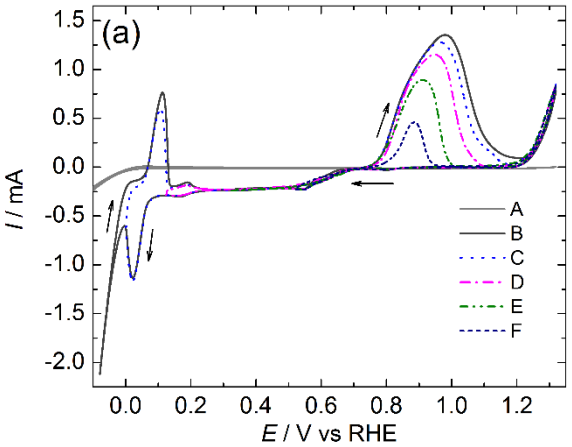
Here, we report a facile synthesis of Pd metallic NPs on Au substrate by electrodeposition from a surfactant-free green electrolyte. The growth modes of Pd NPs were analysed in detail and correlated with their electrocatalytic performance. The electrolyte consisted of $PdCl_2$ as the precursor ion source in an aqueous and mild acidic environment at room temperature allowing sufficient time to form a ligand stabilised coordinated complex $[PdCl_4]^{2-}$, in which Pd^{2+} ions were stabilised by the ligand effects of Cl^- ions, or H_2O or both depending on the electrolyte pH. The effects of the applied overpotential and deposition duration were systematically investigated for their influence on the nucleation, growth and size of the Pd NPs, while other parameters such as precursor concentration and pH of the electrolyte were kept constant. A large potential window positive of the underpotential deposited hydrogen (H_{UPD}) was obtained for the electrodeposition of Pd through the pH dependent ligand coordination effects of Cl^- and H_2O with Pd^{2+} ions and, therefore, Pd NPs at a specific pH were deposited with a little influence of the H_{UPD} on growing Pd nuclei.

2. Results and Discussion

2.1. Electrochemical deposition of Pd

The CV of the Au(111) textured substrate was recorded in deaerated perchlorate ($HClO_4$) electrolyte containing chloride (Cl^-) ions. The behaviour of CV (Figure S3a) is similar to the Au(111) surface and the peaks in the anodic scan corresponds to the structural transition of the Au(111) surface as discussed in the supplementary section. The (111) texture of the substrate was also confirmed by XRD analysis as discussed in section 3.3. The CV in Figure 1a shows a wide onset potential region 0.7-0.27 V_{RHE} for Pd deposition well positive of the underpotential deposited hydrogen (H_{UPD}) region which is found below 0.27 V_{RHE}. A cathodic current due to the reduction reaction 1 (below) started to flow around 0.7 V_{RHE}, followed by a substantial current rise to a maximum at 0.02 V_{RHE} near the diffusion limited reduction of $[PdCl_4]^{2-}$. No cathodic peaks for the underpotential deposition of Pd were observed. In another experiment, CV for the Pd deposition was conducted at slower scan rate of 1 mV s^{-1} from the same electrolyte (Figure S3b). The deposition peaks were similar to that of the higher scan rate and no cathodic peaks due to the underpotential deposition appeared at the potential more positive than 0.7 V_{RHE}. The current of Pd deposition (Figure 1a) decreases sharply beyond the peak at 0.02 V_{RHE} as the mass transfer diffusion dominates, and reaches a minimum at -0.002 V_{RHE} followed by an increase due to the bulk hydrogen evolution. The potential region of 0.7-0.27 V_{REH} is where the Pd metal deposition occurs without H_{UPD} and after this point deposition occurs simultaneously with H_{UPD} on the freshly deposited Pd. As the cathodic potential limit gradually increases into the H_{UPD} region, an anodic current due to Pd stripping at 0.98 V_{RHE} increases i.e., stripping current is linearly proportional to the overpotential indicating the deposition of Pd within the selected potential window. A pair of peaks (C_1, A_1) appears (Figure 1b) as a result of the H adsorption (H_{ads}) and desorption (H_{des}), respectively, when voltammogram (D) was scanned negatively to 0.12 V_{RHE}. As the cathodic potential was scanned into and beyond the H_{UPD} region, a sharp anodic peak appears at 0.11 V_{RHE} (voltammetry B and C) due to H absorption (H_{abs}) onto the Pd lattice and its re-oxidation. In this overpotential region i.e. from 0.27 until -0.08 V_{RHE}, Pd deposition occurs simultaneously with H_{UPD} as indicated by the appearance of a hydrogen desorption peak at 0.11 V_{RHE} along with a larger Pd stripping peak at 0.98 V_{REH} in the anodic scan. The higher anodic peak current for Pd striping indicates that Pd deposition increases as the overpotential increases and is not hindered by the H_{UPD}. The higher cathodic current in the reverse scan for the potential region of 0.48-0.27 V_{RHE} shown in Figure 1b supports the fact that the deposition of Pd on Pd surface is faster than the nucleation on Au electrode surface.

$$[PdCl_4]^{2-} + 2e^- \rightarrow Pd(0) + 4Cl^- \qquad (1)$$



Accepted Manuscript

This article is protected by copyright. All rights reserved.

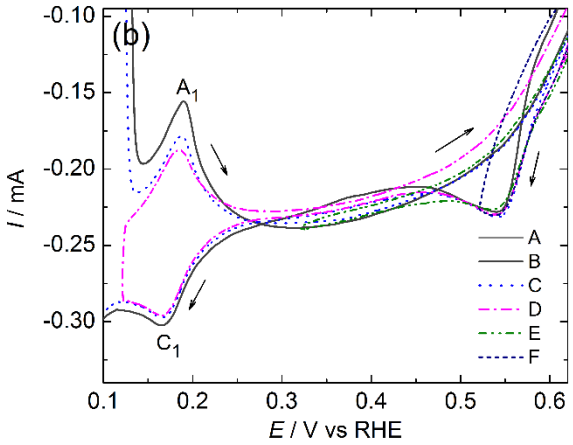


Figure 1. (a) Cyclic voltammetry of the Au substrate recorded in deaerated 0.1 mol L^{-1} HCl electrolyte containing 0.001 mol L^{-1} $PdCl_2$ scanned negatively from OCP with a scan rate of 5 mV s^{-1} (initial/conditioning: 0.79 V_{RHE}, 10 s), the upper potential limit was selected at 1.3 V_{RHE} and reverse potential at 0.52 V_{RHE} (F), 0.32 V_{RHE} (E) 0.12 V_{RHE} (D), -0.002 V_{RHE} (C) and -0.08 V_{RHE} (B), where A represents the voltammogram of the substrate in 0.001 mol L^{-1} HCl electrolyte and (b) Expanded current densities within the selected potential region 0.1 to 0.6 V_{RHE}.

Three overpotentials were selected for the Pd deposition and named as small (0.54 V_{RHE}), medium (0.16 V_{RHE}) and large (-0.002 V_{RHE}) overpotential. The nucleation and growth of Pd at these selected overpotentials was investigated by potentiostatic transient measurement, in which Pd was deposited in a short pulse width of 5 s and stripped at 1.0 V_{RHE}, a potential sufficiently positive to ensure that no Pd remain on the surface. The current-time transients in Figure 2a shows an initial drop in cathodic current due to the adsorption and multistep charge transfer reactions and pass through a minimum to obtain the constant current values at longer deposition times.[18] The last part of the current-time transient was used to plot steady-state current vs. inverse square root of the time in Figure 2b since there is an important contribution of the adsorption current at the beginning of the deposition i.e. short time deposition. The resulting current-time transients recorded for the small, medium and large deposition potentials, all show the characteristic shape for an electrochemically driven, mass-transfer diffusion controlled (i.e., current is proportional to $t^{-1/2}$ at long times), nucleation and growth process.[19] The cathodic current is consistent with the Cottrelian decay indicative of the planar diffusion controlled growth. Thus, the selected overpotential region (i.e., small, medium and large overpotential) is large enough to overcome the potential barrier to nucleate the stable Pd nuclei for further growth.

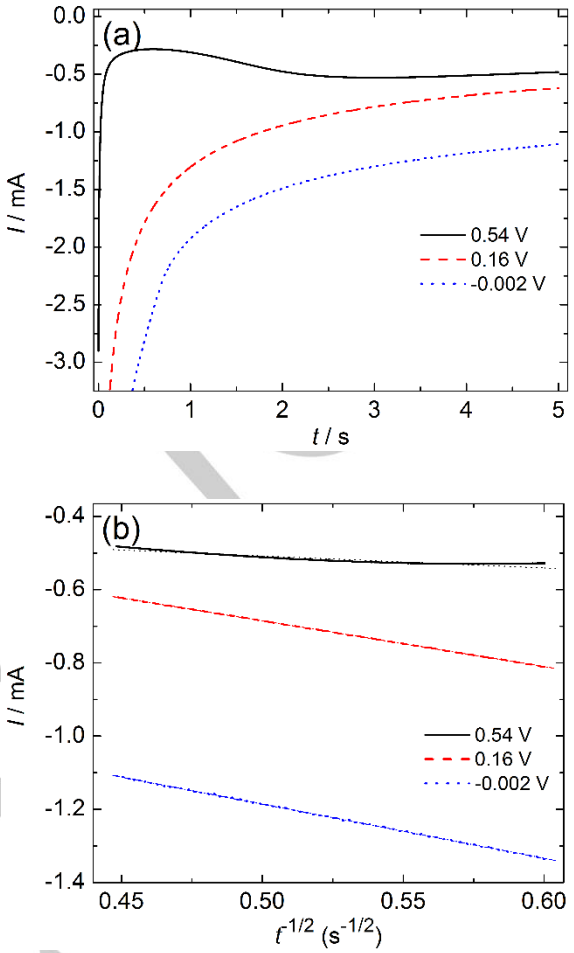


Figure 2. (a) Current-time transient recorded at various overpotentials vs. RHE on a Au substrate in deaerated 0.1 mol L^{-1} HCl electrolyte containing 0.001 mol L^{-1} $PdCl_2$ (initial/conditioning: 0.79 V_{RHE}, 10 s), (b) Plot of current vs. time$^{-1/2}$ showing linear characteristic consistent with the Cottrell equation (see supplementary section). The legend shows the corresponding Pd deposition potential at small 0.54 V_{RHE} (solid line), medium 0.16 V_{RHE} (dash line) and large -0.002 V_{RHE} (dot line).

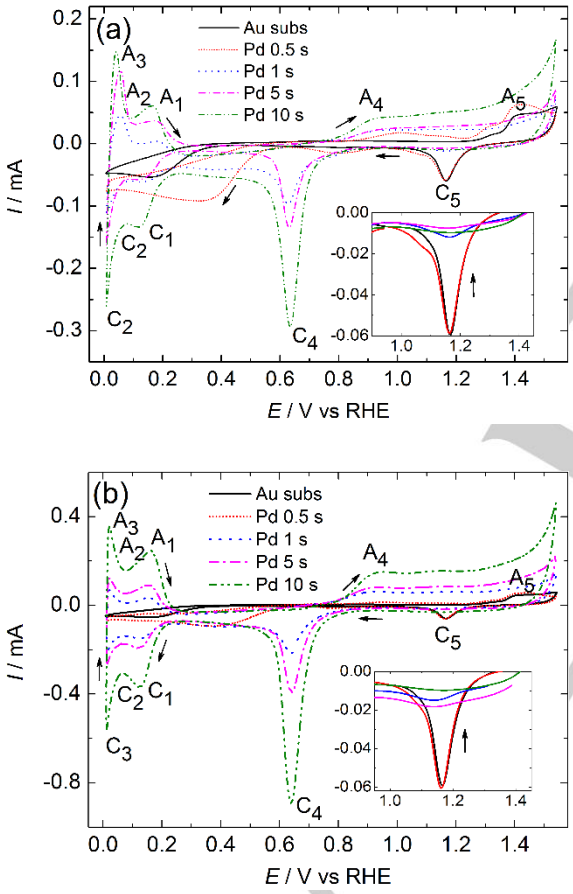
2.2. Characterisation of Pd deposits by cyclic voltammetry in aqueous acidic electrolyte

Figure 3 shows CVs of the Au (111) electrode recorded in 0.1 M H_2SO_4 electrolyte at 20 mV s^{-1} after Pd was deposited potentiostatically at (a) 0.54 V_{RHE} (small overpotential), (b) 0.16 V_{RHE} (medium overpotential) and (c) -0.002 V_{RHE} (large overpotential) for different deposition times. The CVs for all Pd electrodes show the characteristic peaks (C_4, A_4) for Pd oxide reduction (PdO_{red})/formation (Pd_{oxi}) at around 0.64/0.92 V_{RHE} and peaks (C_1, C_2 and A_1, A_2) for H_{UPD} i.e., adsorption (H_{ads}), absorption (H_{abs}) and desorption (H_{des}), respectively, in the potential range 0.2-0.06 V_{RHE}. A pair of peaks (C_3, A_3) represents the bulk process of hydrogen absorption/evolution and re-oxidation from the surface of the Pd at potential 0.01 V_{RHE} or more. A pair of broader peaks (C_5, A_5) at around 1.16 V_{RHE} and 1.4 V_{RHE} corresponds to the Au oxide (Au_2O_3) reduction and formation,

Accepted Manuscript

This article is protected by copyright. All rights reserved.

respectively, are suppressed when the deposition time was more than 0.2 s. The peak corresponding to the reduction of Au_2O_3 was no longer detected as the deposition time increased (insets in Fig. 3) suggesting that the Au surface was fully covered by the Pd deposits and no Au surface remained exposed to the electrolyte. The shape of the CVs in the H_{UPD} region is similar to those obtained at pseudomorphic Pd layers deposited on Au(111) and Au(100) substrates,[20] which indicate that Pd was deposited epitaxially. The peak current due to PdO_{red}/Pd_{oxi} (C_4, A_4), H_{ads}/H_{abs} and H_{des} (C_1, C_2 and A_1, A_2), bulk hydrogen absorption/re-oxidation (C_3, A_3) and oxygen evolution (at larger than 1.5 V_{RHE}) from Pd surfaces increases with increase in the deposition time (see Figure 3 and S4), which indicates that surface roughness of the Pd deposits increases with the deposition time. However, deposition was likely to be low at small overpotential (0.54 V_{RHE}) for longer deposition duration i.e., current for H_{ads}/H_{abs} and H_{des} and PdO_{red} increased slightly with increasing the deposition time as shown in Figure S4.



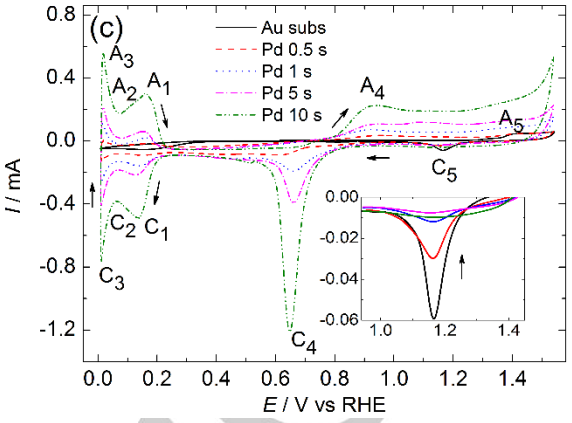


Figure 3. Cyclic voltammetry of the Pd deposited on a Au substrate at (a) 0.54 V_{RHE}, (b) 0.16 V_{RHE} and (d) -0.002 V_{RHE} in deaerated 0.1 M H_2SO_4 electrolyte shows H_{ads}/ H_{abs}/H_{des} as well as Pd oxide formation/reduction peaks. CVs were recorded in static conditions with a scan rate of 20 mV s^{-1} (initial/conditioning: 0.9 V_{RHE}, 10 s) and inset shows the expanded current for the reduction of AuO. The legend indicates the corresponding Pd deposition time.

To examine the nature of the halo-aqua Pd^{2+} complex, UV-visible spectrophotometric analysis was carried out. The UV-visible absorption spectra (Figure 4a) of the electrolyte (0.1 mol L^{-1} HCl electrolyte containing 0.01 mol L^{-1} $PdCl_2$) are similar to those reported in the literature, which is a spin-forbidden d-d transition ($^1A_{2g} \leftarrow {}^1A_{1g}$) of square-planar Pd^{2+} complexes in the range between 350-500 nm.[21] The maximum absorption of the band shifts to shorter wavelengths when the Cl^- ligands are exchanged for H_2O ligands on going from a highly acidic to a lower acidic electrolyte, which is in agreement with the spectrochemical series of the ligands.[21] The maximum absorption peak of the band at 432 nm is given by the coordinated complex $[PdCl_3][H_2O]^-$, in which Cl^- ligands exchanged for H_2O ligands of the complex $[PdCl4]^{2-}$ (assigned absorption peak at 467 nm) and the complex is stabilised by charge transfer from ligands to the central Pd^{2+} ions.[21-22] On further hydrolysis of $PdCl_3][H_2O]^-$ towards a near neutral electrolyte, more Cl^- ligands are displaced by H_2O to produce complexes such as $[PdCl_{4-x}][H_2O]_x^{(x-2)}$ (x = 0-4) [21]. These complexes show a larger shift of the Pd^{2+} d–d transition band to shorter wavelengths (420 nm) and a change in colour of the electrolyte to brown as shown in the inset of Figure 4a. After 10 times dilution to 0.001 mol L^{-1} $PdCl_2$, the maximum absorption peak of the band did not show a wavelength shift (Figure 4b), which confirmed that concentration of the active ions in the electrolyte doesn't affect the coordination nature of the complexes.

Accepted Manuscript

This article is protected by copyright. All rights reserved.

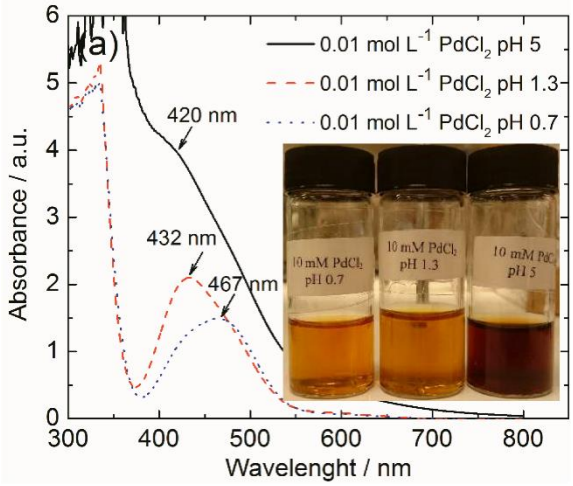


Figure 4. UV-visible absorption spectra of 0.1 mol L^{-1} HCl electrolyte containing (a) 0.01 mol L^{-1} $PdCl_2$ at pH 0.7, 1.3 and 5; (b) comparison between 0.001 and 0.01 mol L^{-1} concentration of Pd^{2+} ions at pH 1.3. Inset: Colour changes of 0.1 mol L^{-1} HCl containing 0.01 mol L^{-1} $PdCl_2$ with increase pH.

2.3. Growth mode and structural characterisation of Pd NPs

Following the deposition of Pd from the aforementioned electrolyte by the potentiostatic pulse at various overpotentials, Pd NPs were observed in an ex-situ examination of the electrode surface using a high resolution FEG-SEM. Figure 5 shows ex-situ FEG-SEM of the different sizes of Pd NPs grown on Au surface where the deposition charge was controlled to 433 μC cm^{-2} (1 monolayer Pd = 440 μC cm^{-2})[23] for each potential. The nanoparticles are grown by direct electrochemical reduction of $[PdCl_4]^{2-}$ ions from the electrolyte on the Au surface according to equation 1. The nanoparticles are randomly dispersed and spherical in shape, in which a large fraction of the substrate is unoccupied. The unoccupied space accounts for the planar diffusion controlled growth of the nuclei as the deposition progresses. The mean particle diameter and distribution were determined by measuring the sizes of at least 1500 particles. The mean diameter of particles deposited at small, medium and large overpotential are 3.8 nm (σ = 1.8), 2.8 nm (σ = 1.2), and 3.5 nm (σ = 1.7), respectively. The average particles size were determined as described in the experimental section 2.3 (also, see the related description in Figure 6 and S5 for more details). It is observed from those measurement that particle sizes vary slightly at each overpotential i.e., dependent on the applied overpotential. The obtained result implies that the average cluster size becomes smaller with higher overpotential for the same deposition time i.e., higher density of nuclei at higher overpotential leads to a smaller average size.

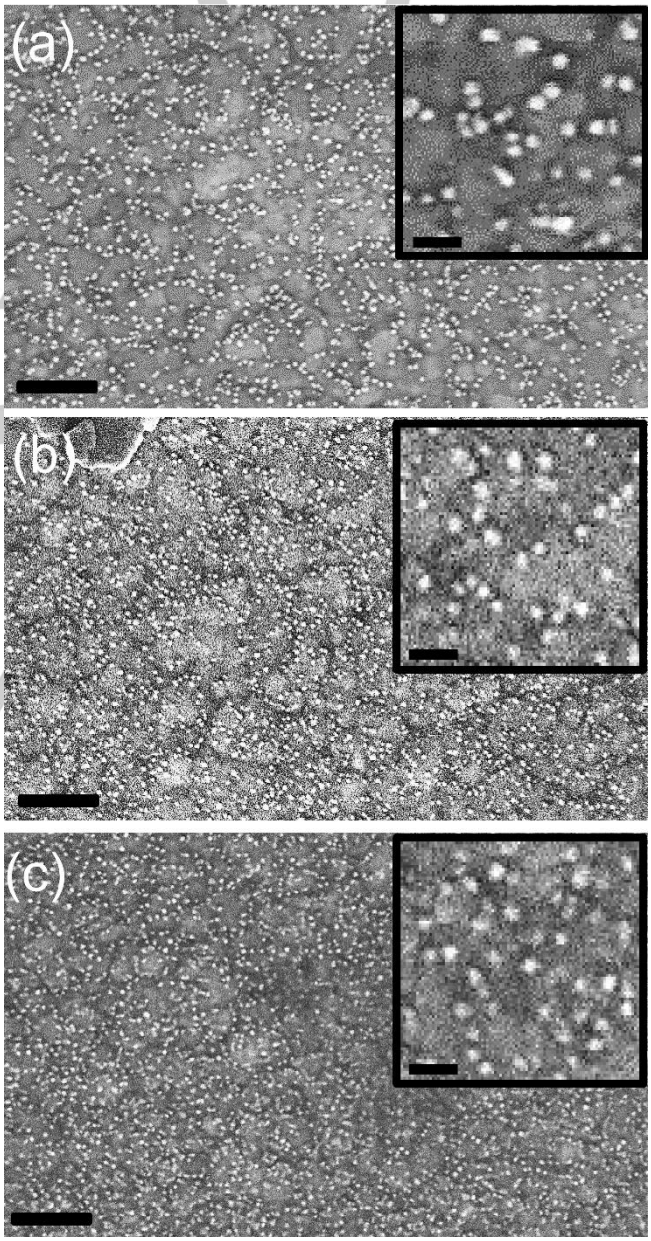


Figure 5. Ex-situ FEG-SEM images for Pd nucleation and growth on a Au substrate electrodeposited potentiostatically at (a) 0.54 V_{RHE}, (b) 0.16 V_{RHE} and (d) -0.002 V_{RHE} for a 433 μC cm^{-2} deposition charge (0.98 monolayer equivalent).

Accepted Manuscript

This article is protected by copyright. All rights reserved.

Inset corresponds to a high magnification FEG-SEM image. Scale bars in the big panel and in the inset are 100 nm and 20 nm, respectively. The electrolyte was made up with deaerated 0.1 mol L^{-1} HCl electrolyte containing 0.001 mol L^{-1} $PdCl_2$.

The growth of Pd NPs was further examined by increasing the amount of Pd deposition charge. A higher amount of Pd deposition charge 3183 μC cm^{-2}, which is 7.3 times larger than that of Figure 5, was controlled potentiostatically on each electrode and representative FEG-SEM images are shown in Figure 6. Pd NPs gradually cover the whole Au surface with a high degree of monodispersity as the deposition progressed. There seems to be a general tendency to increase in size and broaden the size distribution of the nanoparticles as the deposition continues based on the inset profile in Figure 6. The mean diameter of the particles are also increased as the deposition progressed from 3.8 nm to 5.5 nm (σ = 3.1), 2.8 nm to 4.8 nm (σ = 2.4) and 3.5 nm to 5.0 nm (σ = 2.9) for small, medium, and large overpotential, respectively. Hence, the particles size is relatively big at small overpotential compared to that of the large overpotential deposition. According to the particles density figure (Figure S6), the count for the maximum mean diameter particles at small (0.54 V_{RHE}) and medium (0.16 V_{RHE}) overpontential increased by two and three times, respectively, with increasing deposition charge whereas the density of these particles decreased by half in the case of large (-0.002 V_{RHE}) overpotential deposition. In accordance with the particles density character (Figure S6) and inset profile (Figure 6), this phenomena endorses the fact that particles size distribution became more homogeneous with increasing the deposition charge i.e., small clusters of nuclei or particles grew faster than their larger counterpart to attain a comparatively homogeneous distribution of particles during large overpotential deposition. According to the FEG-SEM images discussed above firstly, nuclei and clusters of nuclei are formed randomly on the Au surface; secondly, new clusters are also formed all over the surface as the deposition proceeded; and thirdly, stable clusters are grown by the direct reduction of $[PdCl_4]^{2-}$ ions towards a full coverage of the substrate as the deposition continued. A schematic model for the electrochemical nucleation and growth of Pd deposition at small, medium and large overpotential based on the FEG-SEM results discussed above is shown in Figure 7. The monodispersed Pd nanoparticle are formed without and with a little or large interaction of H_{UPD} on the growing nuclei of Pd and seemingly, H_{UPD} didn't obstruct the growth of the deposits.

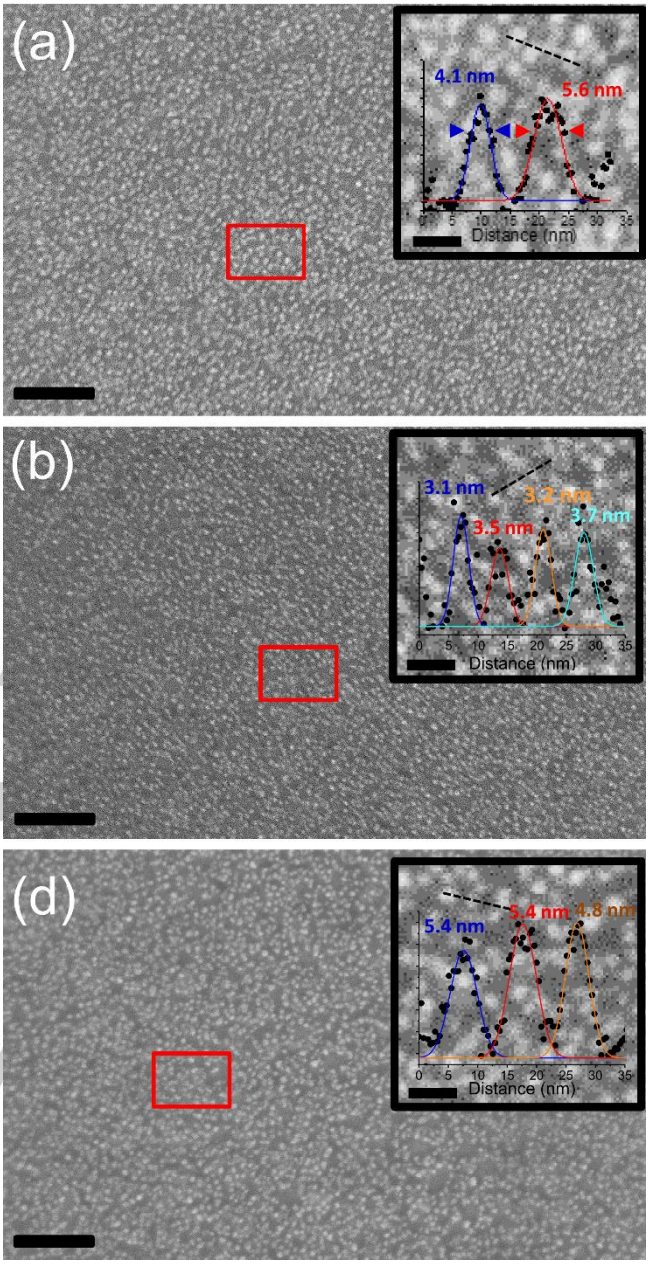


Figure 6. Ex-situ FEG-SEM images of the Pd NPs on a Au substrate electrodeposited potentiostatically at (a) 0.54 V_{RHE}, (b) 0.16 V_{RHE} and (d) -0.002 V_{RHE} for a 3183 μC cm^{-2} deposition charge. The electrolyte was made up with deaerated 0.1 mol L^{-1} HCl electrolyte containing 0.001 mol L^{-1} $PdCl_2$. Insets show the higher magnification images of the areas within the red rectangles, in which examples of profile plots are shown. Dashed black lines represent the cuts where the profiles were analysed. To illustrate the variation in particle sizes, Gaussian fits were performed, the FWHM values of which are noted next to the profiles. Scale bars in the big panel and in the inset are 100 nm and 20 nm, respectively.

Accepted Manuscript

This article is protected by copyright. All rights reserved.

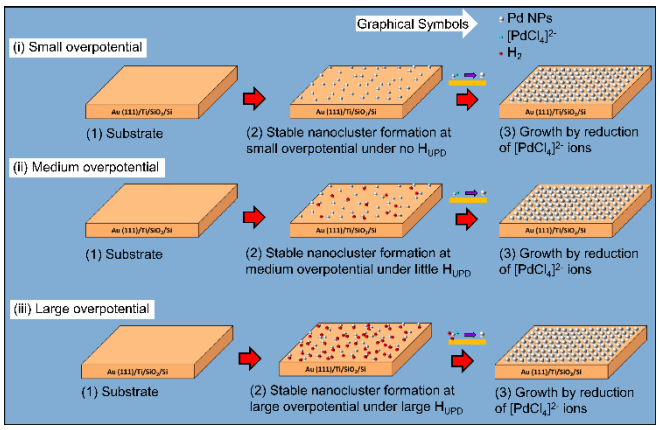


Figure 7. Schematic illustration of the electrochemical growth mechanism of the Pd deposition on a Au substrate when the overpotential is (i) small with no interaction of H_{UPD}, (ii) medium with a little interaction of H_{UPD}, and (iii) large with a significant interaction of H_{UPD}, on the growing nuclei.

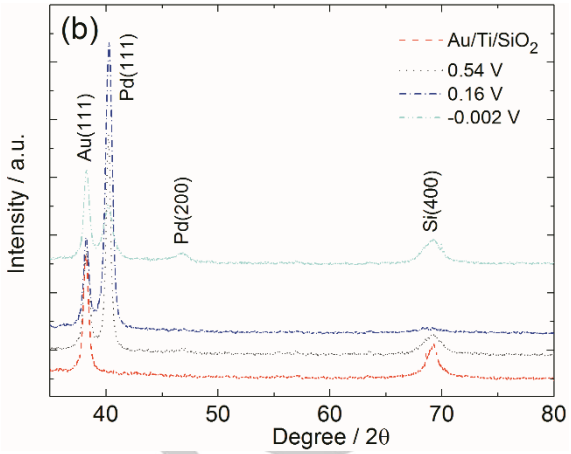
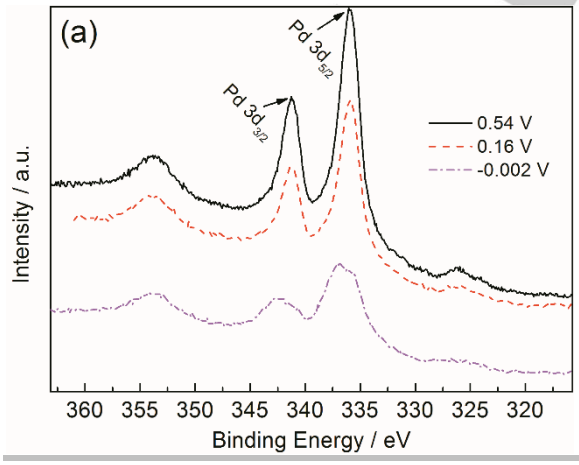


Figure 8. (a) XPS and (b) XRD of Pd NPs on a Au substrate for a total deposition charge of 3183 μC cm^{-2}. The legend shows the corresponding Pd deposition potential at small 0.54 V_{RHE}, medium 0.16 V_{RHE} and large -0.002 V_{RHE}.

The elemental composition, chemical and electronic states of Pd NPs at the Au (111) interface were investigated by XPS as shown in Figure 8a for a deposition charge of 3183 μC cm^{-2}, similar to the deposition charge for which FEG-SEM is shown in Figure 6. Survey scans were carried out initially on a contaminant free Au (111) surface. The survey showed that all the samples contain O, C and Pd photoelectron peak consistent with the modification of the Au surface with Pd NPs. Pd NPs on the gold surface were prepared by applying various potentials while maintaining the same deposition charge. Hence, Au substrate modified with Pd nanoparticles has spin orbit doublets with Pd $3d_{5/2}$ and Pd $3d_{3/2}$ peaks at 335.8 eV and 341.3 eV, respectively. The latter observation seems to be the same for all the electrodes regardless of the applied potential during Pd deposition. That means that there was not any binding energy shift, a fact which indicates that the deposited metallic Pd NPs are pure or contaminant-free. To investigate the crystal structure of Pd NPs, XRD measurements were performed as shown in Figure 8b. A strong diffraction peak was observed, which can be assigned to the (111) face-centred cubic (fcc) structure of metallic Pd along with a tiny peak for the (200) facet.



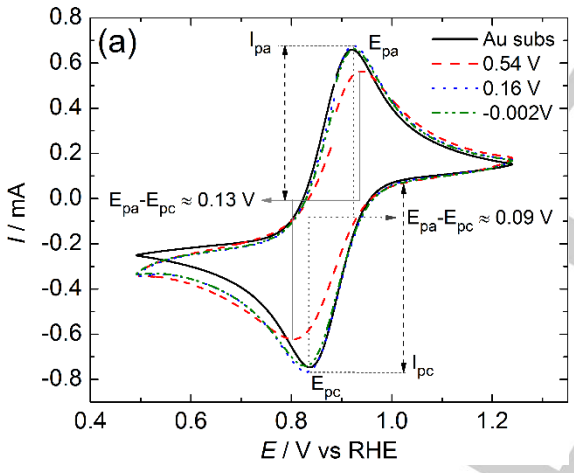
2.4. Electrocatalytic performance measurement of Pd NPs

CVs for the Pd NPs based electrode (corresponding ex-situ FEG-SEM images were shown in Figure 5 and 6) were recorded for the ferrocyanide ($[Fe(CN)_6]^{4-}$)/ferricyanide ($[(Fe(CN)]^{3-}$) system. The peak-to-peak separation (ΔE_p) between the redox couple of the ferrocyanide/ferrocyanide CVs complies with that of the standard curve as discussed in the supporting information section (Figure S7) and demonstrates a quasi-reversible one-electron redox behaviour at the Pd NPs as shown in Figure 9. Before examining the redox behaviour in the above electrolyte, the deposited Pd NPs were electrochemically cleaned in 0.5 mol L^{-1} KOH electrolyte by CV technique. Because it is a surfactant-free Pd NPs surface (as confirmed by XPS in Figure 8a), steady-state CVs were achieved after a few cycles. The redox current of Pd NPs deposited at medium (0.16 V_{RHE}) and large (-0.002 V_{RHE}) overpotential as shown in Figure 9a, is similar to that of the Au substrate (I_{pa} = 0.67 mA and I_{pc}= 0.76 mA) with an anodic (E_{pa})-cathodic (E_{pc}) peak potential separation ($\Delta E_p = E_{pa} - E_{pc}$) of 0.09 V, which indicates faster electron transfer kinetics. However, peak separation of Pd NPs deposited at small (0.54 V_{RHE}) increased to 0.13 V with a slight decrease in the corresponding redox current (I_{pa} = 0.56 mA and I_{pc}= 0.62 mA). This behaviour is due to the partial hindrance of ($[Fe(CN)_6]^{4-}$)/ ($[(Fe(CN)_6]^{3-}$) redox reaction on the Pd NPs surface and slower electron transfer kinetics that leads to a lower current and higher peak separation. However, Pd NPs deposited at small overpotential, whose particles size are quite large by comparison with those deposited at medium and large overpotential might have less activated surface area for redox reaction. As the deposition proceeds, nanoparticles or clusters grew further through the fresh reduction of ions into nanoparticles of the homogenous active sites and surface area. As can be seen from the Figure 9b, the redox peak potentials of the ferrocyanide/ferricyanide system are similar for all Pd NPs electrodes irrespective of the overpotential applied when deposited for longer period of time (corresponding FEG-SEM image is shown in Figure 6). The anodic and cathodic peak

Accepted Manuscript

This article is protected by copyright. All rights reserved.

potential for all Pd NPs are observed at 0.95 V_{RHE} and 0.86 V_{RHE}, respectively, and the corresponding anodic-cathodic peak potential separation ($\Delta E_p = E_{pa} - E_{pc}$) is 0.09 V. The obtained ΔE_p value for Pd NPs is similar with the value of the Au substrate (ΔE_p = 0.09 V), but it should be borne in mind that the Au particles were deposited under vacuum by a sputtering technique, which affords high purity blanket deposits but is more expensive by comparison with the electrodeposition method. A small ΔE_p value obtained for Pd NPs indicates that a good reversibility and electrochemical activity are maintained on the Pd nanoparticles surface.[19a] The redox current of Pd NPs varies slightly with each overpotential applied for their deposition, which are I_{pa} = 0.80 mA and I_{pc} = 0.85 mA (small overpotential), I_{pa} = 0.75 mA and I_{pc} = 0.80 mA (medium overpotential), and I_{pa} = 0.77 mA and I_{pc} = 0.85 mA (large overpotential). The ratio of the cathodic to anodic current is close to 1, suggesting that the reaction undergoes a quasi-reversible redox process. The redox currents for Pd nanoparticles are 1.1 to 1.2 times higher than that of the Au substrates i.e., a larger electrochemically activated surface area of the electrodeposited Pd NPs and faster electron transfer kinetics by comparison with the sputtered Au. The redox current for Pd NPs complied with the theoretically calculated value (0.825 mA) from Randles-Sevcik equation, in which a lower value for the Au substrate can be interpreted in terms of the lower activated surface area for the redox reaction.



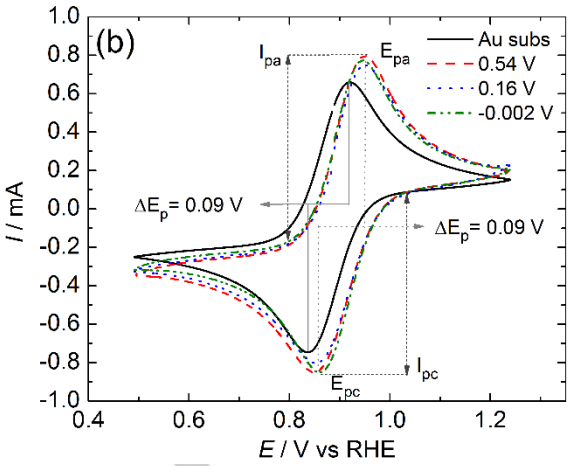


Figure 9. Cyclic voltammetry of Pd NPs on a Au substrate (a) 433 µC cm^{-2} (corresponded SEM is shown Figure 4) and (b) 3183 µC cm^{-2} (corresponded SEM is shown in Figure 5) recorded in deaerated 0.005 mol L^{-1} $K_3[FeCN]_6$ and 1 mol L^{-1} KCl electrolyte. CVs were recorded in static conditions with a scan rate of 50 mV s^{-1} (initial/conditioning: 0.9 V_{RHE}, 10 s).

Pd NPs were characterised by CV in deaerated 0.5 mol L^{-1} KOH aqueous electrolyte as shown in Figure 10. These CVs show similar characteristic features to those reported in the literature for hydrogen adsorption (C_2, C_3) and desorption (A_2, A_3), oxide formation (A_1) and reduction (C_1).[24] The pre-peak (A'_1) and (C'_1) are associated with the oxidation and reduction of the Pd NPs surface, respectively, before the main process occurs. The electroactive surface area (EASA) was calculated from Pd oxide reduction (PdO_{red}) peak at 0.63 V_{RHE} after subtraction of the charge for a double layer charging capacitance. A conversion factor of 424 µC cm^{-2} was used corresponding to the removal of a full monolayer of Pd oxide. The specific surface area (SSA) of the Pd NPs in m^2/g was defined as the EASA of the Pd NPs (cm^2/cm^2 Au substrate) divided by the amount Pd loading. These data are summarised in Table 1 along with the electrocatalytic activity for ethanol electrooxidation in aqueous alkaline electrolytes.

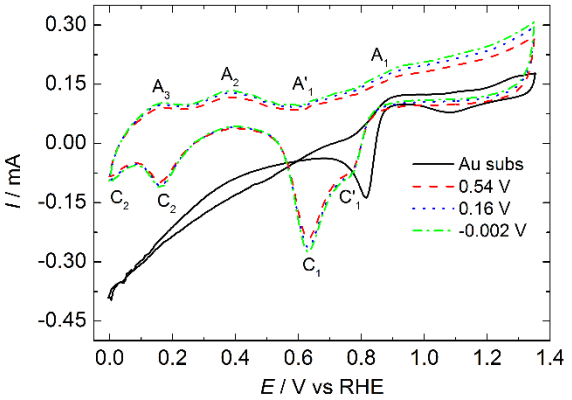


Figure 10. Cyclic voltammetry of Pd NPs deposited on a Au substrate recorded in deaerated 0.5 mol L^{-1} KOH aqueous electrolyte. CVs were recorded in static conditions with a scan rate of 20 mV s^{-1} (initial/conditioning: 1.0 V_{RHE}, 10 s).

Accepted Manuscript

This article is protected by copyright. All rights reserved.

Each electrode contains a total Pd deposition charge of 3183 μC cm^{-2} (i.e., 1.75 x 10^{-6} g cm^{-2}).

Table 1. Overpotential dependent electroactive surface area (EASA), specific surface area (SSA), ethanol electrooxidation and mass activity of Pd NPs at 293K. The specific activity was normalised to the EASA of Pd. The activities were measured at the forward peak potential.

V_{RHE} for Pd NPs deposition	Pd loading g cm^{-2} x 10^{-6}	EASA cm^2(Pd) cm^{-2} (subs)	SSA m^2 g^{-1}(Pd)	Ethanol electrooxidation current specific activity mA cm^{-2}(subs)	mA cm^{-2}(Pd)	Mass activity mA g^{-1}(Pd) x 10^6	I_f/I_b
0.54	1.73	1.58	91.32	17.33	10.96	10.02	0.86
0.16	1.67	1.62	97.00	18.70	11.54	11.20	0.95
-0.002	1.64	1.64	100.00	19.79	12.07	12.07	1.05

The specific surface area (SSA) of Pd NPs deposited at all overpotentials at a nearly similar mass loading varies only slightly for each deposit. However, this difference can be attributed to the particle size and counts of the smallest particles as shown in particles density character (Figure S6). The lowest SSA value (91.32 m^2 g^{-1}) for Pd NPs deposited at 0.54 V_{RHE} is due to comparatively larger particle size (i.e., 5-8 nm with maximum counts for 5.5 nm NPs) effect while the highest values 97.00 m^2 g^{-1} and 100.00 m^2 g^{-1} for the Pd NPs deposited at 0.16 V_{RHE} and -0.002 V_{RHE}, respectively, is due to the combined effects of smaller particles size (2-8 nm) with the maximum counts for only 5 nm Pd NPs. The SSA values of our electrochemically deposited Pd NPs are remarkably higher than the values for electrodeposited nonporous Pd (60 m^2 g^{-1}),[25] Pd coated CNT (25.8 m^2 g^{-1}),[26], Pd nanowires synthesised by electron beam irradiation of a precursor mixture (12 m^2 g^{-1})[27] and Pd black (17-23 m^2 g^{-1}).[28] However, of note is the deposition charge of Pd at -0.002 V_{RHE} may include small amount of H_{UPD} charge which is in the range of H_{UPD} and thus, measured SSA value for Pd NPs is an indicative, which was expected to be higher if H_{UPD} charges were subtracted. On the other hand, small and medium overpotential both are positive of H_{UPD} and thus, calculated SSA values for Pd NPs deposited at those overpotential are accurate.

The electrocatalytic performance of Pd NPs as anode catalysts for alkaline direct alcohol fuel cells (ADAFCs) was evaluated by electrooxidation of ethanol, one of the highest energy density and largely scalable production fuels from the fermentation of biomass. Typical CVs for electrooxidation of ethanol on Pd NPs and the Au substrate electrode in alkaline electrolyte are shown in Figure 11a. Ethanol electrooxidation exhibited two well-defined current peaks, the first at 0.8 V_{RHE} on the forward scan under anodic conditions and the second at 0.68 V_{RHE} on the reverse scan under cathodic conditions. It is clearly seen that the forward and reverse peaks for all Pd NPs electrode are sharper with a higher electrooxidation current by comparison with the substrate Au electrode. The peak on the forward scan is attributed to the electrooxidation of the freshly chemisorbed ethanol species on the Pd NPs and the peak on the reverse scan is caused by the oxidation of the incompletely oxidised carbonaceous species e.g., $(CH_3CO)_{ads}$, formed during the dissociative adsorption of ethanol on the Pd during the forward scan.[29],[30] The formation of the oxide layer can block the adsorption of the new reactive species on the Pd surface and eventually lead to the decrease in the electrocatalytic activity. As the anodic scan continues more Pd oxide covers the surface of the Pd NPs and therefore, the current for the electrooxidation of ethanol is decreased at 0.9 V_{RHE} and no current flows thereafter as the scan is continued. The electrode reactivates again in the reverse scan once the oxide is removed from the Pd NPs surface giving a second oxidation peak at 0.68 V_{RHE}.[30-31] The forward scan onset potential refers to the overpotential required for the electrooxidation of ethanol and it is seen that current started to flow for all Pd NPs electrodes at an overpotential ca. 0.32 V_{RHE}, which is about 0.33 V more negative than the Au substrate (0.65 V_{RHE}). This fact indicates that the stripping reaction of the dissociative adsorbed intermediates $(H_3CO)_{ads}$ of ethanol on the Pd NPs commences at a more negative potential than that of Au. The stripping reaction is known to be the rate determining step for the electrooxidation of ethanol on Pd electrocatalyst in alkaline electrolyte as reported in our previous work.[30] Therefore, electrooxidation of ethanol in alkaline electrolyte is kinetically more favourable on Pd NPs than on Au.

Accepted Manuscript

This article is protected by copyright. All rights reserved.

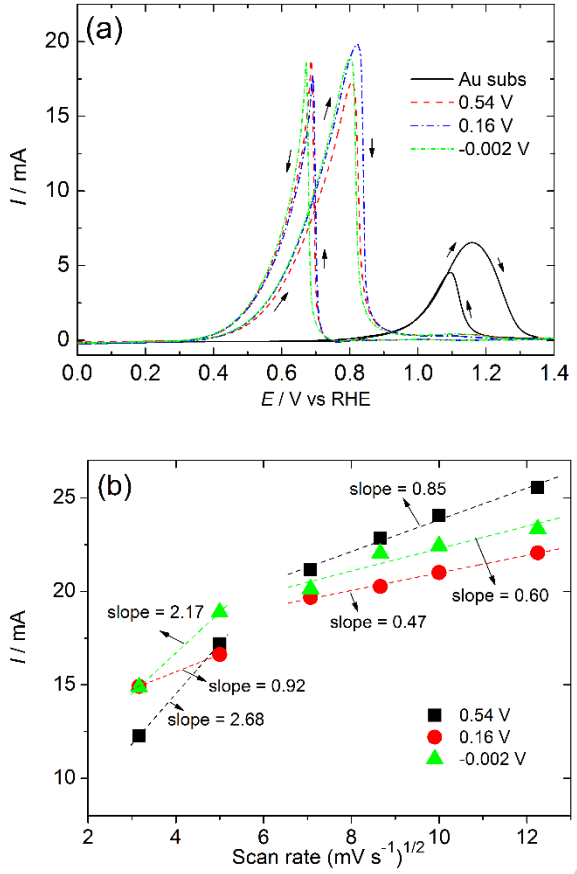


Figure 11. Cyclic voltammetry of Pd NPs deposited on a Au substrate for the electrooxidation of ethanol in deaerated 1 mol L^{-1} ethanol and 0.5 mol L^{-1} KOH electrolyte. CVs were recorded in static conditions with a scan rate of 25 mV s^{-1} (initial/conditioning: 0.4 V_{RHE}, 10 s). Each electrode contains total Pd deposition charge of 3183 µC cm^{-2} (i.e., 1.75 x 10^{-6} g cm^{-2}).

The forward peak potential and corresponding peak current density for electrooxidation of ethanol do not vary significantly between the three Pd NPs electrodes. Although, the EASA value for the three Pd NPs electrodes does not differ much, it is generally accepted that a higher EASA would have more active sites for the electrooxidation of ethanol. The highest electrooxidation current obtained for Pd NPs deposited at -0.002 V_{RHE} corresponded to a specific activity of 12.07 mA (Pd) followed by 11.54 mA (Pd) and 10.96 mA (Pd) for Pd NPs deposited at 0.16 V_{RHE} and 0.54 V_{RHE}, respectively, as the former electrode has a slightly higher EASA value than the latter. This phenomenon is related with the presence of defect sites on Pd NPs surface as described by Ustarroz et. al.[32]

It is known that the electrocatalytic properties of the Pd NPs are influenced by their crystalline structure, particle size and distribution as well as the surface morphology. The normalised specific activities corresponding to the amount of Pd loading is also remarkably high as presented in Table. The enhanced electrocatalytic performance of ethanol electrooxidation mass activity (≈ 10,000 mA mg^{-1}) of our electrochemically deposited Pd NPs is about 13, 10.5, 10.8 and 35 times higher than the corresponding activity reported for Pd nanoflowers/Ni nanowires electrode (765 mA mg^{-1}),[30] $Pd_{45}Pt_{55}$ nanowires on glassy carbon electrode (950 mA mg^{-1}),[33] Pd/rGO/carbon fibre paper (925 mA mg^{-1})[34] and commercial Pd-C/CFP(286 mA mg^{-1}),[34], respectively. As the ethanol electrooxidation on the forward scan occurs under diffusion control, the mass transport behaviour on Pd NPs catalysts has been investigated. Figure 11b shows the correlation between the peak current density (in the forward scan) and the square root of the scan rate during the electrooxidation process of ethanol at different scan rates. The electrooxidation current of ethanol has a linear relationship at different scan rates with two slope values; the first at lower scan rate with a larger value and the second at higher scan rate with a smaller value. This observation indicates that the electrooxidation process of ethanol on Pd NPs was controlled by concentration polarisation or diffusion processes at higher scan rates of above 25 mV s^{-1}. At lower than 25 mV s^{-1} scan rate, the electrooxidation was dominated by the activation polarisation of the Pd NPs over the diffusion electrochemistry. The ratio of the forward anodic peak current density (I_f) to the backward anodic peak current density (I_b) is an important index to measure the tolerance to carbonaceous oxidative intermediates accumulated on the catalyst surface during the electrooxidation of ethanol. A high I_f/I_b ratio implies the effective oxidation of ethanol to the end products and low accumulation and/or effective elimination of carbonaceous oxidative intermediates on/from the electrocatalyst surface.[29] The I_f/I_b ratio of Pd NPs in this work is between 0.86 to 1.05, comparable with the commercial Pd-C catalyst and other reported values.[34] However, the method developed in this work for electrochemical deposition of highly dispersed Pd NPs could be transferred to alternative substrates, which provide faster electron transfer and mass transport by comparison with the Au substrate of this work enabling catalysts that are more tolerant to oxidative intermediates. After 50 potential cycles, the electrooxidation current for ethanol on the anodic scan had decreased by only ≈ 3.5%, which means that our electrochemically deposited Pd NPs are active and stable catalysts.

3. Conclusions

This work investigated the electrochemical deposition of Pd metallic NPs on Au(111) substrate in a deaerated 0.1 mol L^{-1} HCl electrolyte containing 0.001 mol L^{-1} $PdCl_2$ without surfactant and additive effects at small, medium and large overpotential. The effects of the applied overpotential and deposition duration on nucleation, growth, size and morphology of Pd NPs were systematically investigated while other parameters such as precursor concentration and electrolyte pH were kept constant. A large potential window positive of underpotential deposited hydrogen (H_{UPD}) was obtained for the electrodeposition of Pd through the pH dependent ligand coordination effects of Cl^- and H_2O with Pd^{2+} ions and, therefore, Pd NPs at a specific pH were deposited with a little influence of the H_{UPD} on growing Pd nuclei. The structural characterisation by means of high resolution FEG-SEM revealed that the electrochemical nucleation occurred

Accepted Manuscript

This article is protected by copyright. All rights reserved.

randomly on Au substrate when the applied overpotential was small (0.54 V_{RHE}), medium (0.16 V_{RHE}) and large (-0.002 V_{RHE}). At these overpotentials, the randomly nucleated and highly dispersed small nuclei or nanoclusters throughout the surface grew independently by the direct reduction of $[PdCl_4]^{2-}$ ions towards the complete coverage of the substrate. The synthesised Pd NPs were monodispersed with a hemispherical shape of an average particle size 2-5 nm and highly pure as examined by XPS, thanks to the surfactant-free electrochemical deposition process. The high dispersibility, lack of organic contaminants and small particle size of the Pd NPs resulted in the largest specific surface area (4 times of commercial Pd-C) and demonstrated high electrocatalytic activity in ferrocyanide/ferricyanide redox and ethanol electrooxidation processes. The mass activity (≈ 10,000 mA mg^{-1}) for ethanol electrooxidation on our electrochemically deposited Pd NPs is about 35 times higher than the corresponding activity on commercial Pd-C (286 mA mg^{-1}) reported to date.[34]

Experimental Section

Materials

Au(111) textured substrates of 10 nm thickness was formed by a sputtering process on a Ti/SiO_2/Si wafer. The underlying layers of Ti (10 nm) and SiO_2 (500 nm) were deposited by a similar physical method on Si wafer to improve the adhesion of Au and to create an electrical conductivity barrier with the semiconducting Si, respectively. For discussion purposes, we refer to the electrode as a Au substrate only. The wafer was diced into 15 mm x 5 mm pieces and a diced coupon with the area of 0.6 cm^2 (12 mm x 5 mm) was immersed in the electrolyte for deposition. The remaining 3 mm at the top of the coupon was left for electrical connection to the potentiostat. Diced Au electrodes were cleaned in isopropyl alcohol by sonication for 1 hour and dried with N_2 gun prior to each of the Pd deposition experiments. The reagent grade palladium chloride ($PdCl_2$), potassium hexacyanoferrate ($K_3[FeCN]_6$) and potassium chloride (KCl) were purchased from Sigma Aldrich and used as received. The hydrochloric acid (HCl) of 37% was purchased from Fisher Scientific and used as received without further purification.

Electrochemical Characterisation

Cyclic voltammetry (CV) at 5 mV s^{-1} was employed to study the reduction kinetics of $[PdCl_4]^{2-}$ from an aqueous electrolyte consisting of 0.01 mol L^{-1} $PdCl_2$ and 0.001 mol L^{-1} HCl. Pt wire and Ag/AgCl/saturated KCl were used as the counter and reference electrode, respectively. The potential measured against the Ag/AgCl/saturated KCl were converted to the reversible hydrogen electrode (RHE) scale using the equation $E_{RHE} = E_{Ag/AgCl} + 0.059 \times pH + 0.197$ V. A potentiostatic method was applied to grow Pd NPs from the same electrolyte at pH 1.3. The electrode potential was conditioned and equilibrated at an open-circuit potential (OCP) of ca. 0.79 vs. V_{RHE} for 10 s for each step and then held at the potentials 0.54 V_{RHE}, 0.16 V_{RHE}, 0.06 V_{RHE} and -0.002 V_{RHE} for a chosen period until a certain amount of charge passed through the electrode surface. All electrolytes were prepared in milli-Q water (>18 MΩ cm) and deaerated by nitrogen gas flow for at least 30 minutes in a closed Pyrex electrochemical cell. Followed the electrodeposition, the deposits were promptly rinsed with 18 MΩ deionised (DI) water and dried in flowing N_2. The adsorbed $[PdCl_4]^{2-}$ ions on the Pd NPs surface were removed during CV scans, recorded in a 0.1 mol L^{-1} H_2SO_4 by cycling the potentials negatively from OCP to 0 V_{RHE} with a scan rate of 20 mV s^{-1} until a steady-state voltammogram was recorded (see Figure S1). The mass of the Pd NPs deposited on the Au electrode surface was estimated from the cathodic charges passed during the electrodeposition obtained from Fig. S2b after subtraction the ions absorption contribution (see Figure S2c and related discussion). The electrocatalytic performance of the Pd NPs for ethanol oxidation was determined in a mixture of 0.5 mol L^{-1} KOH and 1 mol L^{-1} ethanol electrolyte by CV scanning negatively from OCP (of ca. 0.4 V_{RHE}) with a scan rate of 25 mV s^{-1}. In this case, Pt wire and Hg/HgO/1 mol L^{-1} KOH were used as the counter and reference electrodes, respectively, and the measured potential was converted to RHE using the following equation $E_{RHE} = E_{Hg/HgO} + 0.059 \times pH + 0.115$ V (calibrated standard potential of Hg/HgOH/1 mol L^{-1} KOH vs. SCE is -0.129 V i.e., 0.244 V - 0.129 V = 0.115 V vs. RHE). The current (mA) was measured in per cm^2 of the electrode surface until otherwise specified.

Physical Characterisation

Scanning Electron Microscopy images were obtained using a high resolution Field Emission Gun–Scanning Electron Microscope (FEG-SEM), LEO Gemini 1525. The images were taken at 400K magnification with an extraction voltage of 15 kV, a working distance (WD) of 5 mm. According to the specification of the system, the resolution achievable is about 2 nm. Size determination of NPs size analysis were made using freely available software ImageJ.[35] To improve the particle detection, the original FEG-SEM image was convolved with a matrix that is sensitive to the edge of the particle. The convoluted image was then converted to a binary format and analysed by the software using the Particle Analysis function (see Fig. S7 for more details). The composition of the deposits was measured by X-ray Photoelectron Spectroscopy (XPS) using an Al Kα (1486.6 eV) X-ray source. XPS data were curve fitted using CasaXPS software using a Shirley background.[36] The C 1s peak was calibrated to 285 eV with the following relative sensitivity factors (R.S.F.): C 1s (1.0), O 1s (2.93) and Pd 3d (16.0). The UV-visible absorption spectra of the electrolyte were measured on Cary 4000 UV-Vis spectrophotometer (Agilent Technologies) in the range of 300 nm to 800 nm equipped with a 1 cm path length plastic cuvette.

Acknowledgements

Authors gratefully acknowledge the financial support received from the Irish Research Council under elevate fellowship programme co-funded by Marie Skłodowska Curie Actions (Grant no. ELEVATEPD/2014/15), W. Khunsin would like to acknowledge Marie Skłodowska Curie Actions fellowship received from the European Union's Seventh Framework Programme (FP7/2007-2013) under REA grant agreement (no. 623424) and S. A. Maier would also like to acknowledge EPSRC Reactive Plasmonics Project (EP/M013812/1) as well as the Lee-Lucas Chair in Physics.

Keywords: Electrodeposition • Palladium • Nanoparticles • Nucleation • Fuel Cell

[1] a) F.-R. Fan, D.-Y. Liu, Y.-F. Wu, S. Duan, Z.-X. Xie, Z.-Y. Jiang, Z.-Q. Tian, *J. Am. Chem. Soc.* **2008**, *130*, 6949-6951; b) K. L. McGilvray, C. Fasciani, C. J. Bueno-Alejo, R. Schwartz-Narbonne, J. C. Scaiano,

Accepted Manuscript

UNDER PEER REVIEW

This article is protected by copyright. All rights reserved.

Langmuir **2012**, *28*, 16148-16155; c) C. Burda, X. B. Chen, R. Narayanan, M. A. El-Sayed, *Chem. Rev.* **2005**, *105*, 1025-1102; d) A. Henglein, *J. Phys. Chem.* **1993**, *97*, 5457-5471.

[2] a) J. Lu, H. Zhang, X. Chen, H. Liu, Y. Jiang, H. Fu, *Adv. Synth. Catal.* **2013**, *355*, 529-536; b) X.-F. Wu, H. Neumann, M. Beller, *ChemSusChem* **2013**, *6*, 229-241.

[3] E. R. Krishna, P. M. Reddy, M. Sarangapani, G. Hanmanthu, B. Geeta, K. S. Rani, V. Ravinder, *Spectrochimica Acta Part A: Molecular and Biomolecular Spectroscopy* **2012**, *97*, 189-196.

[4] a) G. Berhault, L. Bisson, C. Thomazeau, C. Verdon, D. Uzio, *Applied Catalysis A: General* **2007**, *327*, 32-43; b) B. Bridier, D. Karhanek, J. Perez-Ramirez, N. Lopez, *ChemCatChem* **2012**, *4*, 1420-1427.

[5] a) S. B. Kalidindi, H. Oh, M. Hirscher, D. Esken, C. Wiktor, S. Turner, G. Van Tendeloo, R. A. Fischer, *Chem. - Eur. J.* **2012**, *18*, 10848-10856; b) F. Ksar, G. K. Sharma, F. Audonnet, P. Beaunier, H. Remita, *Nanotechnol.* **2011**, *22*, 305609-305609; c) E. C. Vermisoglou, A. Labropoulos, G. E. Romanos, E. Kouvelos, S. Papageorgiou, G. N. Karanikolos, F. Katsaros, N. K. Kanellopoulos, *J. Nanosci. Nanotechnol.* **2010**, *10*, 5971-5980.

[6] a) C.-M. Chang, M.-H. Hon, I.-C. Leu, *ACS Appl. Mater. Interfaces* **2013**, *5*, 135-143; b) J.-M. You, H. S. Han, S. Jeon, *J. Nanosci. Nanotechnol.* **2015**, *15*, 5691-5698.

[7] W. J. Fang, S. H. Tang, P. X. Liu, X. L. Fang, J. W. Gong, N. F. Zheng, *Small* **2012**, *8*, 3816-3822.

[8] a) M. I. Prodromidis, E. M. Zahran, A. G. Tzakos, L. G. Bachas, *Int. J. Hydrogen Energy* **2015**, *40*, 6745-6753; b) N. HeYa, Z. Lei, Q. HaiXia, W. Tao, C. MingXi, Y. Nian, L. LingZhi, X. FuBao, G. JianPing, *J. Power Sources* **2015**, *288*, 160-167; c) M. Shao, *J. Power Sources* **2011**, *196*, 2433-2444; d) E. Antolini, *Energy Environ. Sci.* **2009**, *2*, 915-931; e) H. L. Liao, Z. P. Qiu, Q. J. Wan, Z. J. Wang, Y. Liu, N. J. Yang, *ACS Appl. Mater. Interfaces* **2014**, *6*, 18055-18062.

[9] a) O. Verho, T. Akermark, E. V. Johnston, K. P. J. Gustafson, C.-W. Tai, H. Svengren, M. D. Karkas, J.-E. Backvall, B. Akermark, *Chem. - Eur. J.* **2015**, *21*, 5909-5915; b) J. Yang, D. Wang, H. Han, C. Li, *Acc. Chem. Res.* **2013**, *46*, 1900-1909; c) R. Su, R. Tiruvalam, A. J. Logsdail, Q. He, C. A. Downing, M. T. Jensen, N. Dimitratos, L. Kesavan, P. P. Wells, R. Bechstein, H. H. Jensen, S. Wendt, C. R. A. Catlow, C. J. Kiely, G. J. Hutchings, F. Besenbacher, *Acs Nano* **2014**, *8*, 3490-3497; d) F. Cai, D. F. Gao, H. Zhou, G. X. Wang, T. He, H. M. Gong, S. Miao, F. Yang, J. G. Wang, X. H. Bao, *Chem. Sci.* **2017**, *8*, 2569-2573.

[10] A. C. Chen, C. Ostrom, *Chem. Rev.* **2015**, *115*, 11999-12044.

[11] Z. Aiqin, L. Meng, L. Mi, X. Yuanhua, L. Zhenxing, C. Junli, S. Yuan, Z. Jihong, F. Shaoming, J. Dianzeng, L. Feng, *J. Mater. Chem. A* **2014**, *2*, 1369-1374.

[12] a) P. C. Pandey, R. Singh, *RSC Adv.* **2015**, *5*, 10964-10973; b) M. Ganesan, R. G. Freemantle, S. O. Obare, *Chem. Mater.* **2007**, *19*, 3464-3471; c) V. Mazumder, S. Sun, *J. Am. Chem. Soc.* **2009**, *131*, 4588-4589; d) R. Sato, M. Kanehara, T. Teranishi, *Small* **2011**, *7*, 469-473; e) V. P. Ananikov, N. V. Orlov, I. P. Beletskaya, V. N. Khrustalev, M. Y. Antipin, T. V. Timofeeva, *J. Am. Chem. Soc.* **2007**, *129*, 7252-7253; f) Q. B. Zhang, J. P. Xie, J. H. Yang, J. Y. Lee, *Acs Nano* **2009**, *3*, 139-148; g) M. T. Reetz, M. Maase, *Adv. Mater.* **1999**, *11*, 773-777.

[13] a) K. R. Brown, D. G. Walter, M. J. Natan, *Chem. Mater.* **2000**, *12*, 306-313; b) H. Chen, G. Wei, A. Ispas, S. G. Hickey, A. Eychmueller, *J. Phys. Chem. C* **2010**, *114*, 21976-21981.

[14] X. Xia, S. Xie, M. Liu, H.-C. Peng, N. Lu, J. Wang, M. J. Kim, Y. Xia, *Proc. Natl. Acad. Sci. U. S. A.* **2013**, *110*, 6669-6673.

[15] a) M. T. Reetz, W. Helbig, *J. Am. Chem. Soc.* **1994**, *116*, 7401-7402; b) M. T. Reetz, M. Winter, R. Breinbauer, T. Thurn-Albrecht, W. Vogel, *Chem. - Eur. J.* **2001**, *7*, 1084-1094.

[16] a) H. Y. Ma, B. S. Yin, S. Y. Wang, Y. L. Jiao, W. Pan, S. X. Huang, S. H. Chen, F. J. Meng, *ChemPhysChem* **2004**, *5*, 68-75; b) B. S. Yin, H. Y. Ma, S. Y. Wang, S. H. Chen, *J. Phys. Chem. B* **2003**, *107*, 8898-8904; c) S. X. Huang, H. Y. Ma, X. K. Zhang, F. F. Yong, X. L. Feng, W. Pan, X. N. Wang, Y. Wang, S. H. Chen, *J. Phys. Chem. B* **2005**, *109*, 19823-19830; d) W. Pan, X. Zhang, H. Ma, J. Zhang, *J. Phys. Chem. C* **2008**, *112*, 2456-2461.

[17] M. L. Rodriguez-Sanchez, M. J. Rodriguez, M. C. Blanco, J. Rivas, M. A. Lopez-Quintela, *J. Phys. Chem. B* **2005**, *109*, 1183-1191.

[18] M. Rezaei, S. H. Tabaian, D. F. Haghshenas, *Electrochim. Acta* **2012**, *59*, 360-366.

[19] a) A. J. Bard, L. R. Faulkner, *Electrochemical Methods: Fundamentals and Applications*, John Wiley & Sons, Inc., New York, **2002**; b) M. Rezaei, S. H. Tabaian, D. F. Haghshenas, *Electrochim. Acta* **2013**, *87*, 381-387; c) N. A. Al Abass, G. Denuault, D. Pletcher, *Phys. Chem. Chem. Phys.* **2014**, *16*, 4892-4899.

[20] a) H. Naohara, S. Ye, K. Uosaki, *J. Electroanal. Chem.* **2001**, *500*, 435-445; b) H. Naohara, S. Ye, K. Uosaki, *J. Electroanal. Chem.* **1999**, *473*, 2-9; c) H. Naohara, S. Ye, K. Uosaki, *J. Phys. Chem. B* **1998**, *102*, 4366-4373.

[21] L. I. Elding, L. F. Olsson, *J. Phys. Chem.* **1978**, *82*, 69-74.

[22] L. Espinosa-Alonso, K. P. de Jong, B. M. Weckhuysen, *Phys. Chem. Chem. Phys.* **2010**, *12*, 97-107.

[23] M. Baldauf, D. M. Kolb, *J. Phys. Chem.* **1996**, *100*, 11375-11381.

[24] G. Denuault, C. Milhano, D. Pletcher, *Phys. Chem. Chem. Phys.* **2005**, *7*, 3545-3551.

[25] S. Cherevko, N. Kulyk, C. H. Chung, *Nanoscale* **2012**, *4*, 103-105.

[26] C. T. Hsieh, Y. Y. Liu, Y. S. Cheng, W. Y. Chen, *Electrochim. Acta* **2011**, *56*, 6336-6344.

[27] F. Ksar, G. Surendran, L. Ramos, B. Keita, L. Nadjo, E. Prouzet, P. Beaunier, A. Hagege, F. Audonnet, H. Remita, *Chem. Mater.* **2009**, *21*, 1612-1617.

[28] G. Surendran, F. Ksar, L. Ramos, B. Keita, L. Nadjo, E. Prouzet, P. Beaunier, P. Dieudonne, F. Audonnet, H. Remita, *J. Phys. Chem. C* **2008**, *112*, 10740-10744.

[29] R. Manoharan, J. B. Goodenough, *J. Phys. Chem.* **1992**, *2*, 875-887.

[30] M. Hasan, S. B. Newcomb, J. F. Rohan, K. M. Razeeb, *J. Power Sources* **2012**, *218*, 148-156.

[31] Z. X. Liang, T. S. Zhao, J. B. Xu, L. D. Zhu, *Electrochim. Acta* **2009**, *54*, 2203-2208.

[32] J. Ustarroz, X. Ke, A. Hubin, S. Bals, H. Terryn, *J. Phys. Chem. C* **2012**, *116*, 2322-2329.

[33] C. Zhu, S. Guo, S. Dong, *Adv. Mater.* **2012**, *24*, 2326-2331.

[34] M. Sawangphruk, A. Krittayavathananon, N. Chinwipas, *J. Mater. Chem. A* **2013**, *1*, 1030-1034.

[35] C. A. Schneider, W. S. Rasband, K. W. Eliceiri, *Nat. Methods* **2012**, *9*, 671-675.

[36] L. Ley, D. A. Shirley, R. Pollak, S. Kowalczy, *Phys. Rev. Lett.* **1972**, *29*, 1088-1092.

Accepted Manuscript

This article is protected by copyright. All rights reserved.

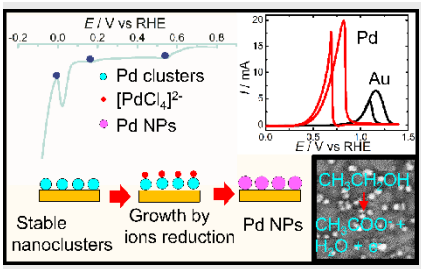
10.1002/celc.201701132

WILEY-VCH

ARTICLE

ARTICLE

Scalable electrochemical synthesis of low dimension Pd nanoparticles (Pd NPs) of below 5 nm with clean surface and high dispersity from a surfactant-free green electrolyte is demonsatrted. The synthesised Pd NPs demonstrated the largest specific surface area (4 times of commercial Pd-C) and the electrocatalytic activity in ferrocyanide/ferricyanide redox and ethanol electrooxidation processes (35 times of Pd-C).



Dr M. Hasan, Dr W. Khunsin C. K. Mavrokefalos, Prof. S. A. Maier, Dr. J. F. Rohan, Prof. J. S. Foord*

Page No. 1–13.

Facile Electrochemical Synthesis of Pd Nanoparticles with Enhanced Electrocatalytic Properties from Surfactant-Free Electrolyte

WILEY-VCH

Accepted Manuscript

This article is protected by copyright. All rights reserved.